Vibrational mode-selective chemistry: Methane dissociation on Ni(100)

Sven Nave and Bret Jackson*
Department of Chemistry, University of Massachusetts, Amherst, Massachusetts 01003, USA
(Received 29 March 2010; revised manuscript received 8 June 2010; published 29 June 2010)

A first-principles full-dimensional model for CH_4 dissociation on Ni(100) is derived using a reaction path formulation. Vibrational excitation of the methane is found to significantly enhance reactivity when the molecule undergoes transitions to the ground or lower-energy vibrational states with the excess energy converted into motion along the reaction path. The ν_1 vibration has the largest efficacy for promoting reaction, with the ν_3 efficacy smaller, but significant.

DOI: 10.1103/PhysRevB.81.233408 PACS number(s): 34.10.+x, 34.35.+a

Elucidating the dynamics of energy flow during a chemical reaction is of great fundamental and practical importance. There has been much recent interest in understanding how vibrational excitation of a molecule can determine or control the outcome of a reaction, and two of the better studied systems in this regard involve reactions of vibrationally excited CH_4, CD_3H, and CD_2H_2 on Ni and Pt surfaces,[1–12] or with Cl in the gas phase.[12–15] We focus here on the dissociative adsorption of CH_4 on a Ni surface, where the molecule breaks a C-H bond as it collides with the metal. This is the rate-limiting step in the important steam reforming reaction, the primary commercial source of H_2. Several groups have measured how the probability for dissociative adsorption varies with both the translational and vibrational energy of the methane.[1–12] The barriers to dissociation are large. Thus, reaction probabilities are small, tunneling can be important, and the reactivity increases strongly with both translational and vibrational energy. Computations place the transition state for dissociation on Ni over a surface atom, with a barrier on the order of 100 kJ/mol that decreases as this atom moves away from the surface, resulting in a significant increase in reactivity with substrate temperature.[16–21] This reaction exhibits nonstatistical behavior with regard to the energy of the incident molecule. For reaction on Ni(100), adding 35 kJ/mol of energy by exciting the symmetric stretch (ν_1) leads to a *greater* increase in reactivity than increasing the translational energy, E_i, by the same amount.[7] These effects are often expressed in terms of a vibrational efficacy,

$$\eta = \frac{\Delta E_i}{\Delta E_v} = \frac{E_i(0,S_0) - E_i(v,S_0)}{\Delta E_v},$$

where ΔE_i is the increase in E_i necessary to give the same reaction probability S_0 as increasing the vibrational energy by ΔE_v. $E_i(v,S_0)$ is the incident translational energy giving a reaction probability S_0 for an initial vibrational state v, where $v=0$ is the ground state. Table I lists experimental efficacies for CH_4 dissociation on Ni(100). For purely statistical behavior, $\eta=1.0$ for all modes. This nonstatistical behavior is not well understood. An early wave-packet study of the nonreactive scattering of oriented CH_4 using model potentials suggested that the efficacy of the ν_1 and ν_3 modes could be larger than for other modes.[22] Halonen *et al.*[23] used a four-dimensional model to examine how the stretching vibrations of CH_4 evolved as the molecule approached a model Ni surface. They predicted a large increase in reactivity with excitation of the ν_1 stretch, and while the asymmetric ν_3 stretch was essentially a spectator mode, estimates of the Massey velocities for curve crossing suggested that nonadiabatic behavior could be important, allowing for energy flow into the reactive C-H bond.

In this study we use a reaction path Hamiltonian (RPH) (Refs. 24 and 25) to examine the dissociation of CH_4 on Ni(100). We include all 15 molecular degrees of freedom within the harmonic approximation, and we compute it from first principles. We recast our RPH into a close-coupled form by expanding the total wave function in the adiabatic vibrational states of the molecule. This allows us to evolve the

TABLE I. Efficacies for the vibrational modes of gas-phase methane with energies E_v. Experimental efficacies η_{ex} for modes ν_3, ν_1, and ν_4 are taken from Refs. 1, 6, and 7. The theoretical efficacies $\eta_{th,1}$, $\eta_{th,2}$, and $\eta_{th,3}$ correspond to the adiabatic case, the inclusion of nonadiabatic coupling to the ground state, and the inclusion of all nonadiabatic coupling, respectively. The η are evaluated at $S_0=10^{-5}$ and averaged over degenerate modes.

Mode	E_v (kJ/mol)	η_{ex}	$\eta_{th,1}$	$\eta_{th,2}$	$\eta_{th,3}$
ν_3	37	0.94	0.03	0.55	0.80
ν_1	36	1.4	0.50	0.87	0.93
ν_2	18		0.09	0.43	0.60
ν_4	15	$\leq$0.5	0.24	0.70	0.71

system and observe transitions between different vibrational states due to the nonadiabatic couplings that arise from the molecule-surface interaction, eliminating the need to estimate transition probabilities or work in a limiting adiabatic representation. We begin by locating the RP, the path of steepest descent from the transition state to the reactant and product states. We do this using electronic-structure methods based on density-functional theory, treating the metal as a four-layer slab. Full details can be found in earlier work.[17–19] Mass-weighted Cartesian coordinates $\{x_i\}$, $i=1,\ldots,15$ describe the location of the five atoms of CH_4 over the rigid metal surface. The distance along the RP is given by s, where $(ds)^2=\Sigma_{i=1}^{15}(dx_i)^2$ and $s=0$ at the transition state. At 68 points along the RP we find the relaxed geometry of the molecule in these coordinates, the total energy, $V_0(s)$, and we perform a normal-mode analysis, computing the normal vibrational coordinates $\{Q_k\}$ and corresponding frequencies $\{\omega_k(s)\}$, $k=1,\ldots,14$, describing motion orthogonal to the RP at that point s, in the harmonic limit. The normal-mode eigenvectors $L_{i,k}(s)$ define the transformation from our $\{x_i\}$ to our RPH coordinates s and $\{Q_k\}$. The resulting (classical) RPH has the form,[25]

$$H=\sum_{k=1}^{14}\left[\frac{1}{2}P_k^2+\frac{1}{2}\omega_k(s)^2Q_k^2\right]+V_0(s)+\frac{1}{2}\left[p_s-\sum_{k=1}^{14}\sum_{j=1}^{14}Q_kP_jB_{k,j}(s)\right]^2\Big/\left[1+\sum_{k=1}^{14}Q_kB_{k,15}(s)\right]^2, \tag{1}$$

where p_s and the $\{P_k\}$ are the momenta conjugate to s and $\{Q_k\}$, respectively, and the vibrationally nonadiabatic couplings are given by

$$B_{k,j}(s)=\sum_{i=1}^{15}\frac{dL_{i,k}}{ds}L_{i,j}(s).$$

When the molecule is far above the surface, only nine of the $\omega_k(s)$ are nonzero, corresponding to the vibrations of gas phase methane. In Fig. 1 we plot these nine frequencies along the RP, labeling them 1–9, in order of decreasing frequency at our first image at large negative s (reactant state). The interaction with the surface removes the degeneracies and significantly softens the ν_1 symmetric stretch (our mode 4) as well as two of the ν_4 bends (modes 8 and 9). There are several avoided crossings. Our only symmetry is a reflection plane lying perpendicular to the Ni surface, and including the C atom and the reacting H atom. The antisymmetric modes 3, 6, and 9 have A'' symmetry (dashed lines), and couple only to each other through the $B_{i,j}$. The symmetric modes have A' symmetry (solid lines) and couple to each other and to the vibrational ground state.

One often assumes vibrational adiabaticity by averaging over the phases of the modes orthogonal to the RP. Following Ref. 25, Eq. (1) becomes

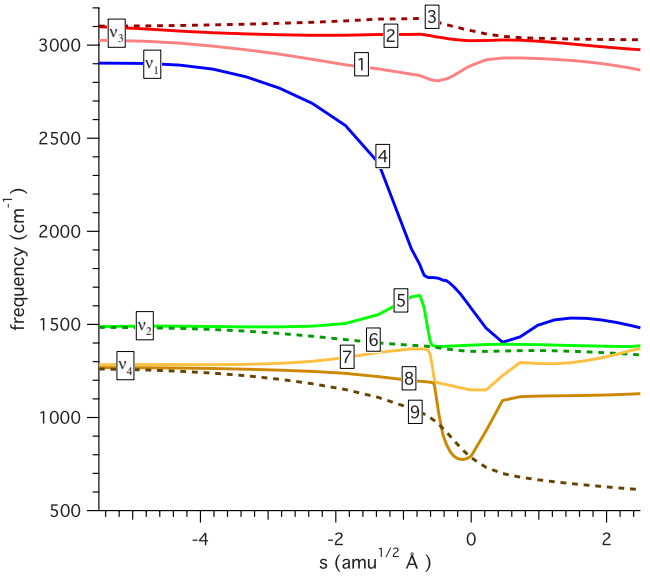

FIG. 1. (Color online) Frequencies of the nine highest-energy normal modes of methane as a function of location along the reaction path.

$$H=\frac{1}{2}A(s)p_s^2+V_0(s)+\sum_{k=1}^{14}\hbar\omega_k(s)\left(n_k+\frac{1}{2}\right)=\frac{1}{2}A(s)p_s^2+V_{eff,\boldsymbol{n}}(s). \tag{2}$$

The one-dimensional effective potentials depend upon the vibrationally adiabatic quantum numbers $\boldsymbol{n}=\{n_k\}$. The mode softening thus leads to a decrease in the effective barrier heights, strongest for modes 4 and 9. The tunneling probabilities through these effective potentials are plotted in Fig. 2. We use the centrifugal-dominant small-curvature semi-

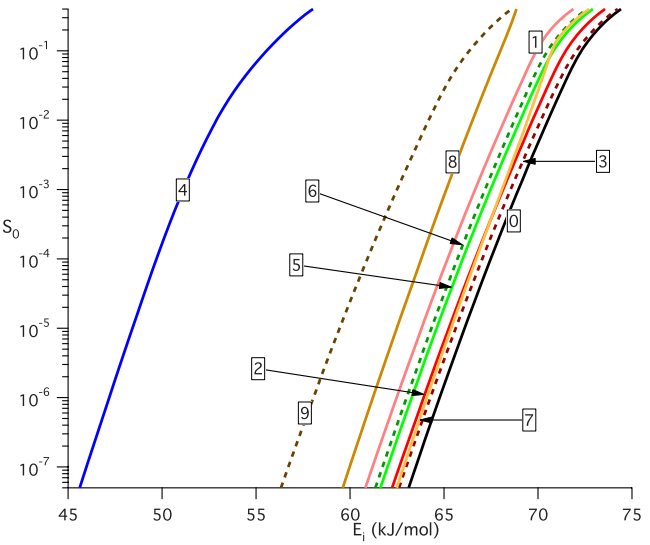

FIG. 2. (Color online) Semiclassical tunneling probabilities as a function of incident energy, for the Hamiltonian of Eq. (1), for methane initially in the ground state (0) or in the first excited state of modes 1–9, as labeled.

classical adiabatic ground-state approach of Truhlar and co-workers[26] to compute $A(s)$, defined by the $B_{i,15}$ terms. This increases reactivity by allowing for tunneling paths away from the RP. As expected, the vibrational efficacies in this vibrationally adiabatic limit, listed in Table I, are small. The dominant effect is the mode softening and thus the ν_1 symmetric stretch has the largest efficacy. Taking into account only the decrease in activation energy due to mode softening, one can approximate η as $[\omega_k(-\infty)-\omega_k(0)]/\omega_k(-\infty)$, which reproduces the computed values well.

The essential physics of the problem, how energy flows between different degrees of freedom, must to a large extent be contained within the harmonic RPH. However, the RPH is complicated and the most general case is difficult to treat quantum mechanically. We recast the RPH into a tractable quantum form by expanding our total wave function in a finite but reasonable space of adiabatic vibrational states $\Phi_{\boldsymbol{n}}$,

$$\Psi(t) = \sum_{\boldsymbol{n}} \chi_{\boldsymbol{n}}(s;t)\Phi_{\boldsymbol{n}}(\{Q_k\};s).$$

These $\Phi_{\boldsymbol{n}}$ are the eigenstates of the first bracketed term in Eq. (1), and depend parametrically upon s. Insertion of $\Psi(t)$ into the time-dependent Schrödinger equation, using the RPH of Eq. (1), leads to a set of coupled equations for the $\chi_{\boldsymbol{n}}(s;t)$. For this initial study we limit our sum over $\boldsymbol{n}$ to include the ground and nine first singly excited vibrational states of the molecule, and our final equations of motion are

$$i\hbar\frac{\partial\chi_0}{\partial t} = \left(\frac{1}{2}p_s^2 + V_{eff,0}\right)\chi_0 - \sum_{v=1}^{9}\left[f_v\frac{\partial^2\chi_v}{\partial s^2} + \frac{df_v}{ds}\frac{\partial\chi_v}{\partial s} + \frac{1}{2}\frac{d^2f_v}{ds^2}\chi_v\right]$$

and

$$i\hbar\frac{\partial\chi_v}{\partial t} = \left(\frac{1}{2}p_s^2 + V_{eff,v}\right)\chi_v - \left[f_v\frac{\partial^2\chi_0}{\partial s^2} + \frac{df_v}{ds}\frac{\partial\chi_0}{\partial s} + \frac{1}{2}\frac{d^2f_v}{ds^2}\chi_0\right] - \sum_{v'=1}^{9}\left[g_{vv'}\frac{\partial\chi_{v'}}{\partial s} + \frac{1}{2}\frac{dg_{vv'}}{ds}\chi_{v'}\right].$$

Our wave packets $\chi_{\boldsymbol{n}}(s;t)$ evolve on the vibrationally adiabatic potentials $V_{eff,\boldsymbol{n}}$ and couple to the other states through the nonadiabatic couplings,

$$f_v(s) = \hbar^2\sqrt{\frac{\hbar}{2\omega_v(s)}}B_{v,15}(s)$$

and

$$g_{vv'}(s) = \frac{\hbar^2}{2}\left[\sqrt{\frac{\omega_{v'}(s)}{\omega_v(s)}}B_{v,v'}(s) - \sqrt{\frac{\omega_v(s)}{\omega_{v'}(s)}}B_{v',v}(s)\right].$$

In the above, $\boldsymbol{n}=0$ denotes the vibrational ground state, and $\boldsymbol{n}=v=1,2,\ldots,9$ labels the nine first singly excited states, using the notation in Fig. 1. Care must be taken in deriving the quantum form of the RPH, as p_s does not commute with the $B_{i,j}(s)$ or $\omega_k(s)$.[27] However, for our single excitation ansatz it is sufficient to expand the RPH to low order in the operators P_k and Q_k, as higher-order terms correspond to higher-order excitations. The parametric dependence of the $\Phi_{\boldsymbol{n}}$ on s leads to nonadiabatic couplings that depend upon the momentum and kinetic energy of the molecule, increasing curve crossing at higher E_i. Standard wave-packet techniques are used to compute the reactive flux, which is Fourier transformed on each channel $\boldsymbol{n}$ to give state- and energy-resolved reaction probabilities.[28]

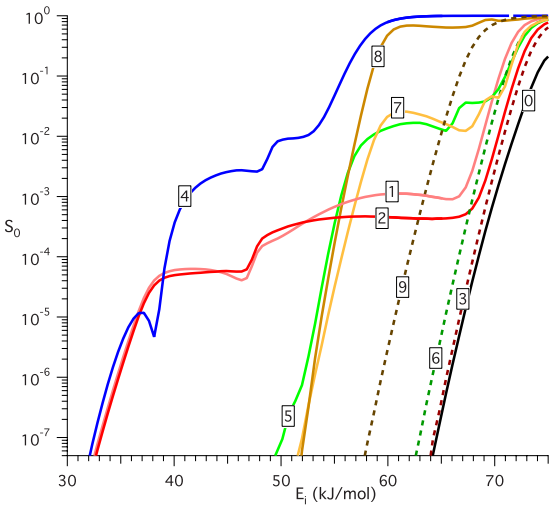

FIG. 3. (Color online) Quantum reaction probabilities as a function of incident energy for methane initially in the ground state (0) or in the first excited state of modes 1–9, as labeled. Only nonadiabatic coupling to the ground state is included.

We first consider, in Fig. 3, the $B_{v,v'}=0$ case, where v and v' span modes 1–9. We include the $B_{v,15}$ terms coupling the A' modes to the ground state and observe several significant effects. First, the ground-state reactivity is lowered relative to the $B_{v,15}=0$ case (not shown) by about a factor of 2. Vibrational excitation competes with dissociation, removing energy from the reaction coordinate. Thus, lower-dimensional models for methane dissociation that ignore "spectator" vibrations overestimate S_0. Second, for modes 3, 6, and 9, where $B_{v,15}=0$ by symmetry, there is only a minor increase in S_0 with vibrational excitation due to mode softening at the transition state. Third, we observe a significant increase in S_0 relative to the adiabatic case for molecules initially excited to the A' modes. This arises from transitions to the ground vibrational state with the excess vibrational energy converted into kinetic energy along the ground-state RP. The structure in Fig. 3 is easy to understand. S_0 decreases rapidly once all classically allowed pathways become closed and tunneling becomes the only reaction mechanism. For molecules initially excited to modes 1 or 2, this drop in reactivity occurs below $E_i=75$ kJ/mol if the molecule remains in the ν_3 state. However, if the molecule undergoes a transition to the ground state, converting vibrational energy into translational energy, this cutoff occurs around 39 kJ/mol. These energies, equal to the difference between the barrier in the final vibrational state, $V_{eff,\boldsymbol{n}}(0)$, and the initial vibrational energy, and can be read off of Fig. 1. For molecules initially excited to the ν_1 symmetric stretch (mode 4), classically allowed processes occur down to $E_i=60$ kJ/mol if the molecule remains in the ν_1 state, or down to 41 kJ/mol if it

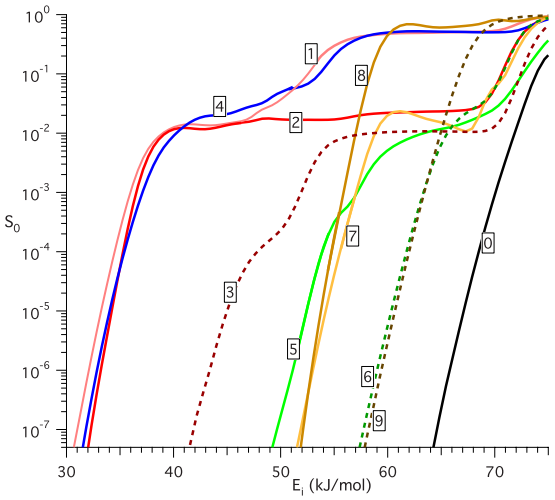

FIG. 4. (Color online) Same as Fig. 3 but all nonadiabatic couplings are included.

scatters to the ground state. For molecules initially excited to modes 5, 7, and 8, over-the-barrier processes via deexcitation to the ground state cease below 58 kJ/mol, 61 kJ/mol, and 61 kJ/mol, respectively. The corresponding η are listed in Table I, and agreement with experiment is improved, relative to the adiabatic case.

We now include all of the couplings, except for $B_{8,7}$ and $B_{7,5}$, as the near degeneracy at these avoided crossings leads to numerical noise. We are exploring ways around this, though preliminary results indicate that their inclusion would not modify our conclusions. The S_0 are plotted in Fig. 4. The addition of new pathways from higher- to lower-energy vibrational states further enhances the reactivity, as the excess energy is converted into translation along the RP. While the A'' modes are not coupled to the ground state or the A' modes, they are coupled to each other. Thus, molecules initially excited to modes 3 and 6 see an increase in reactivity relative to the adiabatic case due to transitions from 3 to 6, 3 to 9, and 6 to 9. The structure in Figs. 3 and 4 have the same origins. For molecules initially excited to mode 3, over the barrier processes cease below about 76 kJ/mol if they remain in this state. If the molecule vibrationally de-excites to mode 6 or 9, over the barrier processes cease below 56 kJ/mol and 49 kJ/mol, respectively. The overall effect of including these extra pathways is to increase the reactivity relative to that in Fig. 3. The η, listed in Table I, are in reasonably good agreement with the ν_1 and ν_3 data. While they are not as large as in the experiments, they are close. Also, the ν_1 mode is the most reactive and the efficacy for the ν_1 mode is larger than for ν_3. The experimental value listed for the ν_4 efficacy is for the triply excited $3\nu_4$ state while our results are the singly excited $1\nu_4$. It is not unreasonable to expect that saturation effects would lower the theoretical efficacy for $3\nu_4$ below 0.71. A more direct comparison with experiment will require a better treatment of the incident wave, an averaging of our results over the velocity and rovibrational distributions in the beam, and a consideration of other reaction paths that might contribute to reactivity.[19] The inclusion of thermal lattice motion can be done using a sudden model, leading to an increase in reactivity.[21] However, we feel that our model captures the essential physics underlying mode-selective chemistry.

B. Jackson gratefully acknowledges support from the Division of Chemical Sciences, Office of Basic Energy Sciences, Office of Energy Research, U.S. Department of Energy under Grant No. DE-FG02-87ER13744.

*Author to whom correspondence should be addressed; jackson@chem.umass.edu

[1] L. B. F. Juurlink, P. R. McCabe, R. R. Smith, C. L. DiCologero, and A. L. Utz, Phys. Rev. Lett. **83**, 868 (1999).
[2] J. Higgins *et al.*, J. Chem. Phys. **114**, 5277 (2001).
[3] M. P. Schmid, P. Maroni, R. D. Beck, and T. R. Rizzo, J. Chem. Phys. **117**, 8603 (2002).
[4] R. D. Beck *et al.*, Science **302**, 98 (2003).
[5] R. R. Smith, D. R. Killelea, D. F. DelSesto, and A. L. Utz, Science **304**, 992 (2004).
[6] L. B. F. Juurlink, R. R. Smith, D. R. Killelea, and A. L. Utz, Phys. Rev. Lett. **94**, 208303 (2005).
[7] P. Maroni, D. C. Papageorgopoulos, M. Sacchi, T. T. Dang, R. D. Beck, and T. R. Rizzo, Phys. Rev. Lett. **94**, 246104 (2005).
[8] R. Bisson *et al.*, J. Phys. Chem. A **111**, 12679 (2007).
[9] D. R. Killelea, V. L. Campbell, N. S. Shuman, and A. L. Utz, Science **319**, 790 (2008).
[10] D. R. Killelea *et al.*, J. Phys. Chem. C **113**, 20618 (2009).
[11] A. L. Utz, Curr. Opin. Solid State Mater. Sci. **13**, 4 (2009).
[12] F. F. Crim, Proc. Natl. Acad. Sci. U.S.A. **105**, 12654 (2008).
[13] Z. H. Kim, H. A. Bechtel, and R. N. Zare, J. Am. Chem. Soc. **123**, 12714 (2001).
[14] S. Yoon, R. J. Holiday, and F. F. Crim, J. Phys. Chem. B **109**, 8388 (2005).
[15] J. C. Corchado, D. G. Truhlar, and J. Espinoza-García, J. Chem. Phys. **112**, 9375 (2000).
[16] G. Henkelman, A. Arnaldsson, and H. Jónsson, J. Chem. Phys. **124**, 044706 (2006).
[17] S. Nave and B. Jackson, Phys. Rev. Lett. **98**, 173003 (2007).
[18] S. Nave and B. Jackson, J. Chem. Phys. **130**, 054701 (2009).
[19] S. Nave, A. K. Tiwari, and B. Jackson, J. Chem. Phys. **132**, 054705 (2010).
[20] C. Luntz and J. Harris, Surf. Sci. **258**, 397 (1991).
[21] A. K. Tiwari, S. Nave, and B. Jackson, Phys. Rev. Lett. **103**, 253201 (2009).
[22] R. Milot and A. P. J. Jansen, Phys. Rev. B **61**, 15657 (2000).
[23] L. Halonen, S. L. Bernasek, and D. J. Nesbitt, J. Chem. Phys. **115**, 5611 (2001).
[24] R. A. Marcus, J. Chem. Phys. **45**, 4500 (1966).
[25] W. H. Miller, N. C. Handy, and J. E. Adams, J. Chem. Phys. **72**, 99 (1980).
[26] D.-h. Lu *et al.*, Comput. Phys. Commun. **71**, 235 (1992).
[27] J.-Y. Fang and S. Hammes-Schiffer, J. Chem. Phys. **108**, 7085 (1998).
[28] J. Dai and J. Z. H. Zhang, J. Phys. Chem. **100**, 6898 (1996).